**Chinese Journal of Health Management**
*Volume 20 Issue 3, Year of Publication 2026, Page 714-722 | DoI-10.564220/1674-0815.2026.92*

ISSN: 1674-0815

**Chinese Journal of Health Management**

Chinese Medical Association


# Chitosan-Based Lipid–Polymer Hybrid Nanoparticles of Encorafenib for Improved Intranasal Delivery in Glioblastoma

**Divya Zambre, Dr. Veena S Belgamwar**
Department of Pharmaceutical Sciences, Rashtrasant Tukadoji Maharaj Nagpur University, Nagpur.

***Article Information***
Received: 26-12-2025
Revised: 18-01-2026
Accepted: 23-02-2026
Published: 07-05-2026

**Keywords**
*Glioblastoma, lipid–polymer hybrid nanoparticles (LPHNPs).*

## ABSTRACT:
Glioblastoma is an aggressive brain tumor where effective treatment is often limited by poor drug delivery to the brain. In the present study, chitosan-based lipid–polymer hybrid nanoparticles (LPHNPs) of encorafenib were developed with the aim of improving intranasal delivery. The nanoparticles were prepared using the nanoprecipitation method and evaluated for their physicochemical characteristics, drug release behavior, mucoadhesive properties, ex vivo permeation, and in vitro cytotoxicity. The optimized formulation showed nanosized particles with low polydispersity and a positive surface charge, indicating suitability for nasal delivery. A high entrapment efficiency was achieved, along with a sustained drug release profile following diffusion-controlled kinetics. The formulation exhibited appreciable mucoadhesion and improved permeation across the nasal mucosa compared to the drug solution. Cytotoxicity studies in U87 glioblastoma cells demonstrated enhanced activity of the nanoparticle formulation over the free drug. In addition, histopathological and hemolysis studies indicated good biocompatibility. These findings suggest that the developed LPHNPs have potential as a carrier system for intranasal delivery of encorafenib. Further in vivo studies would be useful to confirm their applicability in glioblastoma treatment.

## 1. INTRODUCTION:
Glioblastoma (GBM) is the most aggressive primary brain tumor, with standard therapy yielding a median survival on the order of only ~12–15 months and long-term survival below 10%[1,2]. Its diffuse invasion and the blood–brain barrier (BBB) severely limit drug delivery to tumor tissue. The BBB excludes >98% of small molecules and nearly all biologic drugs, so even drugs active in vitro often fail in GBM due to poor brain penetration. This challenge has prompted interest in targeted therapies and alternative routes of administration [3]. BRAF mutations (particularly V600E) occur in a minority of GBMs (on the order of ~5–10%) but represent a druggable pathway [4]. Encorafenib is a potent, second-generation BRAF V600E inhibitor (developed for melanoma) that strongly suppresses MAPK signaling and proliferation in BRAF-mutant cancer cells. In melanoma and colorectal cancers, encorafenib is FDA-approved (often combined with a MEK inhibitor) and can induce tumor responses [5]. Early glioma trials suggest that BRAF/MEK inhibitor combinations can yield objective responses even in high-grade

gliomas [6]. However, encorafenib is a substrate for efflux pumps (e.g., P-gp/ABCG2) and its penetration into the brain is limited under normal BBB function [7]. Thus, reformulating encorafenib for nose-to-brain delivery could enhance its local concentration in GBM while minimizing systemic exposure.

Intranasal delivery exploits the unique nasal–olfactory anatomy to bypass the BBB [8]. The nasal mucosa provides "direct entry to the CNS mainly through the sensory neuronal pathway or indirectly by passage across the BBB" [9]. In essence, drugs can travel along olfactory and trigeminal nerves into the brain, avoiding first-pass metabolism and enabling rapid onset of action [10]. For example, intranasal administration of certain neurotherapeutics has produced appreciable cerebrospinal and brain tissue concentrations that would not be achievable via intravenous dosing [11]. Nanoparticle carriers are especially promising in this context as they can protect the drug from nasal enzymes, facilitate mucosal transport, and enhance uptake along neural pathways. Indeed, recent reviews note that nanoparticle-based systems demonstrate an outstanding capacity to overcome challenges of nasal delivery and achieve significant drug accumulation in the brain [9].

Chitosan is a widely used polymer for nasal nanocarriers. Its cationic, mucoadhesive nature prolongs residence time on the nasal mucosa and transiently opens tight junctions, enhancing drug absorption [12]. Chitosan nanoparticles have shown improved brain delivery of various drugs in preclinical studies, often by adsorptive-mediated endocytosis across the olfactory epithelium [13]. Lipid–polymer hybrid nanoparticles (LPHNPs) combine the structural integrity of polymeric NPs with a lipid shell's biocompatibility. LPHNPs are next-generation core-shell nanostructures, conceptually derived from both liposomes and polymeric nanoparticles. The combined design allows high drug loading and sustained release (via the polymer) together with high biocompatibility (via the lipid) [14,15].

Despite advances in intranasal nanodelivery, no prior study has formulated encorafenib as a chitosan-based LPHNP for nose-to-brain GBM therapy. Given encorafenib's poor BBB permeability and the promising results of intranasal nanoparticle carriers in brain disease models, we propose to develop chitosan–lipid hybrid NPs encapsulating encorafenib for intranasal administration. The present work thus focuses on formulating and characterizing encorafenib-loaded LPHNPs (using chitosan and suitable lipid components), optimizing their physicochemical properties (size, charge, drug release), and evaluating ex vivo nasal mucosal permeation and in vitro cytotoxicity against U87 glioblastoma cells. We hypothesize that these mucoadhesive LPHNPs will enhance nasal uptake and drug transport into the CNS, potentially improving the effective dose reaching GBM cells while minimizing systemic exposure. This strategy could address the dual challenges of GBM therapy, the aggressive tumor biology, and the restrictive BBB by repurposing an existing targeted agent (encorafenib) via a nose-to-brain nanocarrier.

## 2. MATERIALS AND METHODS:

### 2.1 Materials:

Encorafenib was obtained as a gift sample from Hetero Drugs Pvt. Ltd., India. Phospholipon® 90G was kindly provided as a gift sample by Lipoid GmbH, Germany. Chitosan (degree of deacetylation ~75%, molecular weight 50–190 kDa) and Poloxamer 407 were procured from Sigma-Aldrich (USA). All other chemicals and solvents used in the study were of analytical grade and used as received without further purification. Distilled water was used throughout the study.

### 2.2 Preparation of Encorafenib-Loaded Chitosan-Based LPHNPs:

Encorafenib-loaded chitosan-based lipid–polymer hybrid nanoparticles (LPHNPs) were synthesized using the nanoprecipitation technique combined with high-shear homogenization [16]. The organic phase was prepared by dissolving encorafenib hydrochloride and Phospholipon 90G in ethanol, while the aqueous phase was consisted of chitosan (solubilized in 1% v/v acetic acid) and Poloxamer 407 (0.5–1% w/v). Nanoparticle formation was achieved through the dropwise addition of the organic phase into the aqueous phase under high-shear homogenization (8000–12000 rpm) for a duration of 10 min. The resulting dispersion was subjected to continuous stirring for 2–3 h to facilitate the complete evaporation of ethanol. Subsequently, the nanoparticles were isolated via centrifugation at 15,000 rpm for 30 min, and the obtained pellet was washed and redispersed in distilled water. Blank nanoparticles were prepared following an identical protocol without the drug.

**2.3 Particle Size, Polydispersity Index, and Zeta Potential:**
The mean particle size, polydispersity index (PDI), and zeta potential of the prepared nanoparticles were analyzed using dynamic light scattering (DLS) (nanopartica SZ-100, Horiba) [17]. The nanoparticle dispersion (1 mL) was diluted with distilled water (10 mL) prior to analysis. All determinations were conducted at a controlled temperature of 25 °C. All measurements were performed in triplicate, and results were expressed as mean ± standard deviation.

**2.4 Morphological Characterization:**
The surface morphology of the optimized LPHNP formulations was analyzed using field emission scanning electron microscopy (FE-SEM). Briefly, a 10 µL aliquot of the sample was mounted onto an aluminum stub using adhesive carbon tape and dried under vacuum, followed by gold sputter coating. Morphological imaging was conducted at an accelerating voltage of 10 kV at appropriate magnifications.

**2.5 Entrapment Efficiency:**
The entrapment efficiency (%EE) of encorafenib-loaded LPHNPs was determined using an ultracentrifugation technique. Briefly, the nanoparticle dispersion was subjected to centrifugation at 15,000 rpm for a duration of 30 min at 4 °C using a cooling centrifuge. The concentration of free drug in the supernatant was subsequently quantified using UV–visible spectrophotometry at the predetermined wavelength.

**2.6 In Vitro Drug Release Study:**
The in vitro drug release of encorafenib-loaded LPHNPs were analyzed using a Franz diffusion cell [18]. Briefly, a dialysis membrane (molecular weight cut-off 12–14 kDa), pre-equilibrated in distilled water, was mounted between the donor and receptor compartments. An accurately measured volume of the nanoparticle dispersion was introduced into the donor compartment, while the receptor compartment consisted of phosphate buffer (pH 6.4), maintained at a controlled temperature of 37 ± 0.5 °C under continuous stirring. At predetermined time intervals, aliquots were withdrawn from the receptor compartment and subsequently replaced with an equivalent volume of fresh medium to maintain sink conditions. The concentration of drug in the collected samples was quantified using UV–visible spectrophotometry (Model UV-1800, Shimadzu, Japan) at the wavelength of 262.5 nm.

**2.7 Drug Release Kinetics:**
The in vitro drug release kinetics of encorafenib-loaded LPHNPs were analyzed using various mathematical models to elucidate the underlying release mechanism. The obtained release data were fitted to zero-order, first-order, Higuchi, and Korsmeyer–Peppas models using DD Solver, a Microsoft Excel add-in program. The mathematical model exhibiting the highest correlation coefficient ($R^2$) was identified as the best-fit model. In the Korsmeyer–Peppas model, the release exponent (n) was utilized to characterize the mechanism of drug release.

**2.8 Mucoadhesion Study:**
The mucoadhesive interaction between the synthesized LPHNPs and mucin was analyzed using a turbidimetric method [19]. Briefly, a mucin dispersion (0.08% w/v) was prepared in distilled water and subjected to continuous stirring overnight to facilitate the formation of a homogeneous solution, followed by centrifugation at 6000 rpm for the removal of undissolved particles. The nanoparticle dispersion was blended with the mucin dispersion in a 2:1 ratio and subjected to vortexing for a duration of 1 min. The turbidity of the resulting mixture was quantified using UV–visible spectrophotometry at a wavelength of 650 nm at predetermined time intervals (0, 30, and 60 min). Mucin dispersion was utilized as a control for all measurements. Additionally, alterations in the mean particle size and zeta potential of the nanoparticle–mucin mixture were analyzed using dynamic light scattering at 0, 30, and 60 min to further elucidate the underlying nanoparticle mucin interactions [20].

**2.9 Ex Vivo Permeation Study:**
Ex vivo permeation studies were performed using freshly excised goat nasal mucosa obtained from a local slaughterhouse. The mucosal tissue was carefully separated and washed with normal saline to remove adhered debris. The permeation study was carried out using a Franz diffusion cell, with the mucosal side facing the donor compartment [21]. The receptor compartment was filled with simulated nasal fluid (pH 6.4) and maintained at 37 ± 0.5 °C under continuous stirring. An accurately measured amount of nanoparticle formulation was placed in the donor compartment. At predetermined time intervals, samples were withdrawn from the receptor compartment and replaced with fresh medium to maintain sink conditions. The samples were analyzed using a UV–visible

spectrophotometer to determine the amount of drug permeated. The cumulative amount of drug permeated was plotted as a function of time. The steady-state flux (J) and permeability coefficient (Kp) were calculated to evaluate permeation behavior.

### 2.10 Hemolytic Toxicity Study:

The hemocompatibility of LPHNPs was evaluated using fresh animal blood. Blood samples were centrifuged to isolate red blood cells (RBCs), which were washed with phosphate-buffered saline (PBS) and diluted to obtain an RBC suspension. The nanoparticle formulations were incubated with the RBC suspension at 37 °C for a predetermined time. Following incubation, samples were centrifuged, and the absorbance of the supernatant was measured using a UV–visible spectrophotometer to quantify hemoglobin release. PBS and distilled water were used as negative (0% hemolysis) and positive (100% hemolysis) controls, respectively [23].
The percentage hemolysis was calculated using the following equation:

$$\%\ Hemolysis = \frac{Absorbance\ of\ Sample}{Absorbance\ of\ 100\%\ lysis} \times 100$$

### 2.11 In Vitro Cytotoxicity Study (MTT Assay):

The cytotoxicity of encorafenib-loaded LPHNPs was evaluated using the MTT assay on U87 cells (procured from NCCS, Pune) [24]. Cells were seeded in 96-well plates at a density of $1 \times 10^4$ cells/well and incubated for 24 h in minimum essential medium (MEM) supplemented with 10% fetal bovine serum (FBS) and 1% penicillin–streptomycin at 37 °C in a humidified atmosphere containing 5% $CO_2$. Following incubation, cells were treated with a range of concentrations (0.1–25 µg/mL for encorafenib and LPHNPs, and 0.001–0.1 µg/mL for paclitaxel). Samples were initially dissolved in DMSO and further diluted with serum-free medium such that the final DMSO concentration did not exceed 0.1% (v/v). Blank nanoparticles were also evaluated to assess formulation-related cytotoxicity. After 24 h of treatment, MTT solution (5 mg/mL) was added and incubated for 2 h. The culture medium was then removed, and the formed formazan crystals were dissolved in dimethyl sulfoxide (DMSO). The absorbance was measured at 540 nm using a microplate reader. Untreated cells served as control, while wells without MTT were considered as blank. The percentage cell viability was calculated, and $IC_{50}$ values were determined from dose–response curves using GraphPad Prism.

## 3. RESULTS AND DISCUSSION:

### 3.1 Formulation Development of LPHNPs:

Various lipid–polymer hybrid nanoparticle (LPHNP) formulations were developed by varying the concentration of chitosan and Poloxamer 407, while maintaining a constant lipid content. In addition, the effect of drug-to-lipid ratio on nanoparticle characteristics was also investigated. The formulations were prepared using the nanoprecipitation method, which is based on rapid diffusion of the organic solvent into the aqueous phase, resulting in spontaneous nanoparticle formation [25]. Chitosan was selected as the polymer due to its mucoadhesive and cationic nature, while the lipid component facilitates the incorporation of the hydrophobic drug within the core [26, 27]. Poloxamer 407 was used as a stabilizer to improve nanoparticle stability and prevent aggregation [28]. The compositions of all formulations are presented in Table 1, and further evaluation was performed based on physicochemical characteristics to select the optimized formulation.

**Table 1. Composition and Physicochemical Characterization of Encorafenib-Loaded LPHNPs**

| Batch | Drug:Lipid | Chitosan (mg) | Poloxamer 407 (mg) | Particle size (nm) | PDI | Zeta Potential (mV) | EE (%) |
|---|---|---|---|---|---|---|---|
| **F1** | 1:5 | 25 | 30 | 187.25 ± 1.5 | 0.32 ± 0.02 | +22 ± 1.5 | 68.4 ± 2.1 |
| **F2** | **1:5** | **50** | **30** | **150.41 ± 0.94** | **0.25 ± 0.01** | **+31 ± 1.2** | **78.6 ± 2.3** |
| **F3** | 1:5 | 75 | 30 | 122.75 ± 1.13 | 0.21 ± 0.01 | +32 ± 1.0 | 74.2 ± 2.0 |
| **F4** | 1:10 | 50 | 30 | 143.47 ± 1.25 | 0.27 ± 0.02 | +29 ± 1.3 | 81.5 ± 2.5 |
| **F5** | 1:5 | 50 | 20 | 165.96 ± 1.26 | 0.30 ± 0.02 | +25 ± 1.4 | 70.3 ± 2.2 |

### 3.2 Particle Size, Polydispersity Index, and Zeta Potential:

The prepared LPHNP formulations were evaluated for particle size, polydispersity index (PDI), and zeta potential, and the results are presented in Table 1. The particle size of the developed formulations ranged from 135 ± 1 nm to 175 ± 1 nm, indicating successful formation of nanoparticles within the nanoscale range suitable for intranasal delivery [29]. An increase in chitosan concentration resulted in a decrease in particle size, which may be attributed to improved stabilization and efficient particle formation during nanoprecipitation, as evident from Figure 1a. The

PDI values ranged from 0.23 to 0.31, indicating a relatively narrow size distribution. However, a slight increase in PDI was observed at lower stabilizer concentration, suggesting reduced stabilization efficiency and increased heterogeneity [28]. The zeta potential of all formulations was found to be positive, ranging from +26.8 ± 1.3 mV to +33.5 ± 1.5 mV, confirming the presence of chitosan on the nanoparticle surface. The increase in zeta potential with increasing chitosan concentration is attributed to the presence of protonated amino groups, which impart a positive surface charge as shown in figure 1b. The obtained particle size and surface charge are favorable for enhanced mucosal interaction and permeation in intranasal delivery systems [30]. Among the formulations, F2 exhibited optimal characteristics, with moderate particle size, low PDI, and sufficiently high zeta potential, and was therefore selected for further studies.

### 3.3 Entrapment Efficiency:

The entrapment efficiency (%EE) of the developed LPHNP formulations is presented in Table 1. The %EE of the formulations ranged from 68.4 ± 2.1% to 81.5 ± 2.5%, indicating efficient incorporation of encorafenib within the lipid–polymer hybrid system. The variation in entrapment efficiency among different formulations can be attributed to differences in polymer and lipid composition. An increase in chitosan concentration from F1 to F2 resulted in improved entrapment efficiency, which may be due to enhanced polymeric network formation and better drug retention. However, a slight decrease in %EE was observed at higher chitosan concentration (F3), which can be attributed to increased viscosity of the polymeric phase, leading to reduced diffusion and inefficient drug encapsulation [31]. Formulation F4, containing a higher drug-to-lipid ratio, exhibited the highest entrapment efficiency, suggesting that increased lipid content enhances the solubilization and retention of the hydrophobic drug within the lipid core [32]. In contrast, formulation F5, with reduced stabilizer concentration, showed comparatively lower entrapment efficiency, which may be due to insufficient stabilization of the nanoparticle system and increased drug leakage. Although F4 exhibited slightly higher entrapment efficiency, formulation F2 was selected as the optimized formulation based on its balanced physicochemical properties, including particle size, polydispersity index, and zeta potential. The overall high entrapment efficiency observed in the developed LPHNPs confirms the suitability of the lipid–polymer hybrid system for efficient delivery of hydrophobic drugs.

### 3.4 Morphological Characterization:

The surface morphology of the optimized LPHNPs (F2) was examined using FE-SEM, as shown in Figure 1c. The nanoparticles appeared as discrete nanosized structures with approximately spherical morphology, confirming the formation of the lipid–polymer hybrid system. A slight degree of aggregation was observed, which may be attributed to particle adhesion during the drying process. The particle size observed in SEM analysis was consistent with the DLS results, confirming nanoscale dimensions of the prepared formulation.

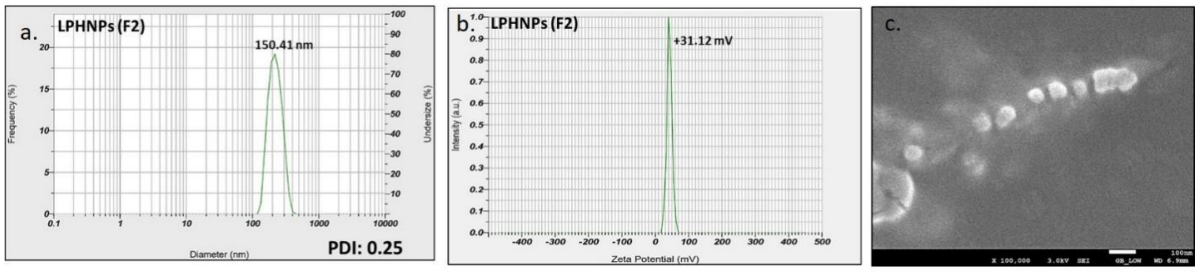


**Figure 1. Characterization of optimized LPHNPs (F2): (a) particle size distribution showing mean diameter of 150.41 nm with PDI of 0.25, (b) zeta potential profile indicating a positive surface charge of +31.12 mV, and (c) FE-SEM image showing spherical morphology of nanoparticles.**

### 3.5 In Vitro Drug Release Study:

The in vitro drug release profiles of encorafenib from drug solution and optimized LPHNPs (F2) are presented in Figure 2a. The drug solution exhibited a rapid release pattern, with approximately 51.65% drug released within 2 h and nearly 97.82% release within 10 h, indicating immediate availability of the drug in the dissolution medium. In contrast, the LPHNP formulation demonstrated a sustained release profile, with only 22.89% drug released at 2 h, followed by a gradual increase to 54.15% at 10 h and 75.50% at 48 h. This release behavior indicates controlled drug release from the nanoparticle system. The initial burst release observed in LPHNPs may be attributed to the release of drug adsorbed on or near the nanoparticle surface, while the subsequent sustained release phase is likely governed by diffusion of the drug from the lipid–polymer matrix. The significantly slower release from LPHNPs compared to the drug solution suggests effective encapsulation of encorafenib within the

hybrid system, which restricts immediate drug diffusion. The presence of chitosan and lipid components contributes to the formation of a dense matrix, thereby controlling drug release. This sustained release profile is advantageous for intranasal drug delivery, as it may enhance drug residence time and improve therapeutic efficacy in glioblastoma treatment [33,34].

### 3.6 Drug Release Kinetics:

The in vitro drug release data were fitted to various kinetic models, including zero-order, first-order, Higuchi, and Korsmeyer–Peppas models, and the results are summarized in Table 2. For the drug solution, the release profile showed the best fit with the first-order model ($R^2$ = 0.9964), indicating concentration-dependent drug release. In contrast, the optimized LPHNPs (F2) exhibited the highest correlation with the Korsmeyer–Peppas model ($R^2$ = 0.9398), suggesting diffusion-controlled drug release from the polymeric matrix. The release exponent (n) value for LPHNPs was found to be 0.361, indicating Fickian diffusion mechanism. This confirms that drug release from the nanoparticles is primarily governed by diffusion through the lipid–polymer matrix. The Higuchi model also showed a good fit ($R^2$ = 0.8773), further supporting diffusion-controlled release behavior. The lower correlation observed with zero-order kinetics indicates that the release is not constant over time. Overall, the kinetic analysis demonstrates that the developed LPHNPs provide a controlled release of encorafenib, governed predominantly by diffusion mechanisms [35,36].

**Table 2: Kinetic modeling parameters of drug release from encorafenib solution and LPHNPs**

| Model | Parameter | Drug Solution (Enco) | LPHNPs (F2) |
|---|---|---|---|
| **Zero Order** | $R^2$ | 0.7011 | 0.1752 |
| | $k_0$ | 12.018 | 2.308 |
| **First Order** | $R^2$ | 0.9964 | 0.8486 |
| | $k_1$ | 0.353 | 0.068 |
| **Higuchi Model** | $R^2$ | 0.9777 | 0.8773 |
| | k_H | 33.107 | 13.687 |
| **Korsmeyer–Peppas** | $R^2$ | 0.9804 | 0.9398 |
| | k_KP | 35.531 | 21.038 |
| | n | 0.461 | 0.361 |

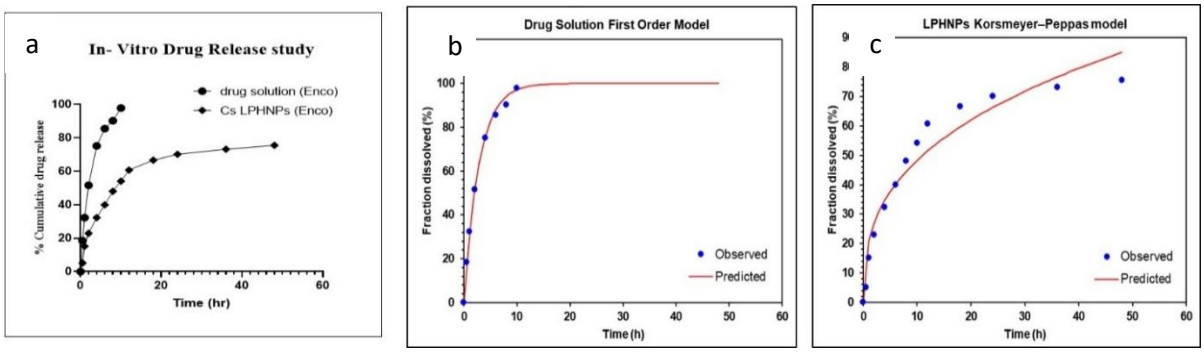


**Figure 2: In vitro drug release and kinetic modeling of encorafenib formulations; (a) Cumulative in vitro drug release profile of encorafenib from drug solution and optimized LPHNPs (F2), (b) First-order kinetic model plot for drug solution showing concentration-dependent release, (c) Korsmeyer–Peppas model plot for LPHNPs (F2) indicating diffusion-controlled drug release.**

### 3.7 Mucoadhesion Study:

The LPHNPs exhibited a mucoadhesion efficiency of 56.63 ± 2.4%, indicating effective interaction with mucin. The time-dependent increase in turbidity upon interaction with mucin is illustrated in Figure 3a, upon incubation with mucin, a noticeable increase in particle size was observed, with the hydrodynamic diameter increasing from 158 nm to 178 nm, suggesting adsorption of mucin onto the nanoparticle surface. Simultaneously, the zeta potential decreased from +32 mV to +19 mV, indicating electrostatic interaction between the positively charged chitosan nanoparticles and negatively charged mucin. This reduction in surface charge further confirms the formation of a nanoparticle–mucin complex. These findings demonstrate that chitosan-based LPHNPs possess significant mucoadhesive properties, which may enhance residence time in the nasal cavity and improve drug absorption for intranasal delivery [26].

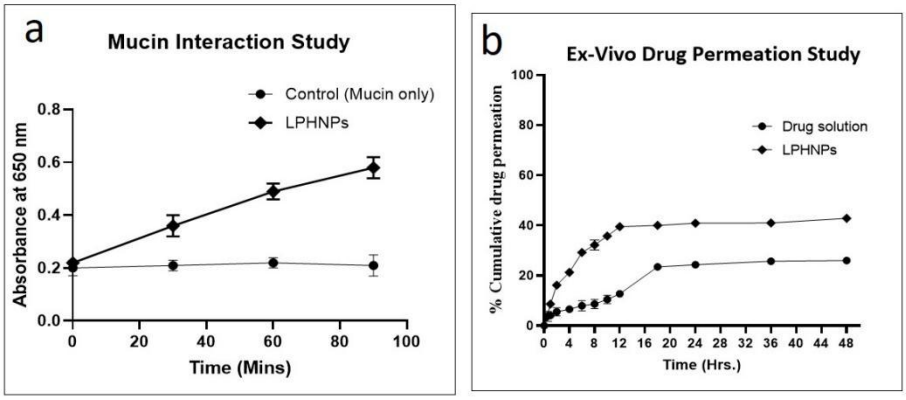


**Figure 3: (a) Time-dependent mucin interaction study showing increased turbidity of LPHNPs compared to control, indicating mucoadhesive behavior. (b) Ex vivo drug permeation profile of encorafenib from drug solution and optimized LPHNPs (F2) across nasal mucosa.**

### 3.8 Ex Vivo Permeation Study:

The cumulative drug permeation profiles are presented in Figure 3b. Drug permeation from LPHNPs was higher compared to the drug solution at all-time points. The drug solution exhibited a gradual permeation, reaching 26.03% at 48 h, whereas LPHNPs showed improved permeation with better drug transport across the nasal mucosa. The steady-state flux (J) of LPHNPs (9.74 µg/cm²/h) was higher than that of the drug solution (8.58 µg/cm²/h). Similarly, the permeability coefficient (Kp) of LPHNPs (0.0487 cm/h) was greater than that of the drug solution (0.0429 cm/h). The enhancement ratio was found to be 1.13, indicating improved permeation of encorafenib from the nanoparticle system. The enhanced permeation may be attributed to the presence of chitosan, which imparts mucoadhesive properties and facilitates transient opening of tight junctions, thereby enhancing paracellular transport [37]. Additionally, the nanoscale size and positive surface charge of LPHNPs promote improved interaction with the nasal mucosa, resulting in enhanced drug absorption. Overall, the developed LPHNPs demonstrated improved permeation of encorafenib compared to the drug solution, supporting their potential for intranasal delivery.

### 3.9 Hemolytic Toxicity Study:

The hemocompatibility of the optimized LPHNPs (F2) was evaluated by measuring the percentage hemolysis of red blood cells. The chitosan-based LPHNPs exhibited minimal hemolysis (1.6%), indicating good compatibility with red blood cells. The observed hemolysis value was well below the 5% threshold for non-hemolytic materials, confirming the safety of the formulation. Microscopic examination further supported these findings, showing intact red blood cell morphology comparable to the negative control, while the positive control exhibited significant cell disruption. These results demonstrate that the developed LPHNPs are hemocompatible and suitable for intranasal drug delivery applications.

### 3.10 In Vitro Cytotoxicity (MTT Assay):

A concentration-dependent decrease in cell viability was observed for both formulations. The LPHNPs exhibited enhanced cytotoxicity compared to the free drug. The $IC_{50}$ value of LPHNPs (2.95 ± 0.10 µg/mL) was lower than that of the free drug (5.51 ± 0.22 µg/mL), indicating improved anticancer efficacy of the nanoparticle formulation. The blank nanoparticles showed negligible cytotoxicity, with cell viability remaining above 90%, confirming the biocompatibility of the developed system. The enhanced cytotoxicity of LPHNPs may be attributed to improved cellular uptake, sustained drug release, and increased interaction with cancer cells.

## 4. CONCLUSION:

In the present study, chitosan-based lipid–polymer hybrid nanoparticles (LPHNPs) of encorafenib were successfully developed and evaluated for intranasal delivery. The optimized formulation exhibited appropriate particle size, narrow size distribution, and positive surface charge, which are favorable for interaction with the nasal mucosa. The formulation showed high drug entrapment along with a sustained release profile, indicating effective incorporation of the drug within the hybrid system. The observed release followed a diffusion-controlled mechanism. Additionally, the nanoparticles demonstrated appreciable mucoadhesive properties and improved permeation across the nasal mucosa, suggesting enhanced residence time and drug absorption. The cytotoxicity

results indicated improved anticancer activity of the nanoparticle formulation compared to the free drug, while safety studies confirmed its biocompatibility. Overall, these findings suggest that chitosan-based LPHNPs can serve as a promising carrier for intranasal delivery of encorafenib. Further in vivo studies are required to validate their potential for glioblastoma therapy.

## 5. REFERENCES:

1. Singh S, Dey D, Barik D, Mohapatra I, Kim S, Sharma M, et al. Glioblastoma at the crossroads: current understanding and future therapeutic horizons. Signal Transduct Target Ther 2025;10:213. https://doi.org/10.1038/s41392-025-02299-4.
2. Parvez A, Rahman MA, Shimki AI, Biswas P, Hasan MH, Imtiaz M, et al. A Comprehensive Analysis of Natural Bioactive Molecules for the Treatment and Control of Glioblastoma Multiforme (GBM) Targeting Underlying Molecular Mechanism. Chem Biodivers 2026;23:e01413. https://doi.org/10.1002/cbdv.202501413.
3. Vargas R, Martinez-Martinez N, Lizano-Barrantes C, Pacheco-Molina JA, García-Montoya E, Pérez-Lozano P, et al. Advancing through the blood-brain barrier: mechanisms, challenges and drug delivery strategies. ADMET DMPK 2025;13:2988. https://doi.org/10.5599/admet.2988.
4. Di Nunno V, Gatto L, Tosoni A, Bartolini S, Franceschi E. Implications of BRAF V600E mutation in gliomas: Molecular considerations, prognostic value and treatment evolution. Front Oncol 2022;12:1067252. https://doi.org/10.3389/fonc.2022.1067252.
5. Sun J, Zager JS, Eroglu Z. Encorafenib/binimetinib for the treatment of BRAF-mutant advanced, unresectable, or metastatic melanoma: design, development, and potential place in therapy. Onco Targets Ther 2018;11:9081–9. https://doi.org/10.2147/OTT.S171693.
6. Arbour G, Ellezam B, Weil AG, Cayrol R, Vanan MI, Coltin H, et al. Upfront BRAF/MEK inhibitors for treatment of high-grade glioma: A case report and review of the literature. Neurooncol Adv 2022;4:vdac174. https://doi.org/10.1093/noajnl/vdac174.
7. Zhang Y, Vagiannis D, Budagaga Y, Sabet Z, Hanke I, Rozkoš T, et al. Encorafenib Acts as a Dual-Activity Chemosensitizer through Its Inhibitory Effect on ABCC1 Transporter In Vitro and Ex Vivo. Pharmaceutics 2022;14. https://doi.org/10.3390/pharmaceutics14122595.
8. Misra SK, Pathak K. Nose-to-brain targeting via nanoemulsion: Significance and evidence. Colloids Interfaces 2023;7:23. https://doi.org/10.3390/colloids7010023.
9. Formica ML, Real DA, Picchio ML, Catlin E, Donnelly RF, Paredes AJ. On a highway to the brain: A review on nose-to-brain drug delivery using nanoparticles. Appl Mater Today 2022;29:101631. https://doi.org/10.1016/j.apmt.2022.101631.
10. Crowe TP, Greenlee MHW, Kanthasamy AG, Hsu WH. Mechanism of intranasal drug delivery directly to the brain. Life Sci 2018;195:44–52. https://doi.org/10.1016/j.lfs.2017.12.025.
11. Chauhan MB, Chauhan NB. Brain Uptake of Neurotherapeutics after Intranasal versus Intraperitoneal Delivery in Mice. J Neurol Neurosurg 2015;2.
12. Mura P, Maestrelli F, Cirri M, Mennini N. Multiple Roles of Chitosan in Mucosal Drug Delivery: An Updated Review. Mar Drugs 2022;20. https://doi.org/10.3390/md20050335.
13. Mikušová V, Mikuš P. Advances in Chitosan-Based Nanoparticles for Drug Delivery. Int J Mol Sci 2021;22. https://doi.org/10.3390/ijms22179652.
14. Gajbhiye KR, Salve R, Narwade M, Sheikh A, Kesharwani P, Gajbhiye V. Lipid polymer hybrid nanoparticles: a custom-tailored next-generation approach for cancer therapeutics. Mol Cancer 2023;22:160. https://doi.org/10.1186/s12943-023-01849-0.
15. Mukherjee A, Waters AK, Kalyan P, Achrol AS, Kesari S, Yenugonda VM. Lipid-polymer hybrid nanoparticles as a next-generation drug delivery platform: state of the art, emerging technologies, and perspectives. Int J Nanomedicine 2019;14:1937–52. https://doi.org/10.2147/IJN.S198353.
16. Mehandole A, Mahajan S, Aalhate M, Kumar R, Maji I, Gupta U, et al. Dasatinib loaded mucoadhesive lecithin-chitosan hybrid nanoparticles for its augmented oral delivery, in-vitro efficacy and safety. Int J Pharm 2024;651:123784. https://doi.org/10.1016/j.ijpharm.2024.123784.
17. Yousaf R, Khan MI, Akhtar MF, Madni A, Sohail MF, Saleem A, et al. Development and evaluation of chitosan and glyceryl monostearate based matrix lipid polymer hybrid nanoparticles (LPHNPs) for oral delivery of itraconazole. Heliyon 2023;9:e14281. https://doi.org/10.1016/j.heliyon.2023.e14281.
18. Awadeen RH, Boughdady MF, Zaghloul RA, Elsaed WM, Abu Hashim II, Meshali MM. Formulation of lipid polymer hybrid nanoparticles of the phytochemical Fisetin and its in vivo assessment against severe acute pancreatitis. Sci Rep 2023;13:19110. https://doi.org/10.1038/s41598-023-46215-8.
19. He P, Davis SS, Illum L. In vitro evaluation of the mucoadhesive properties of chitosan microspheres. Int J Pharm 1998;166:75–88. https://doi.org/10.1016/s0378-5173(98)00027-1.
20. Voci S, Gagliardi A, Giuliano E, Salvatici MC, Procopio A, Cosco D. In Vitro Mucoadhesive Features of Gliadin Nanoparticles Containing Thiamine Hydrochloride. Pharmaceutics 2024;16. https://doi.org/10.3390/pharmaceutics16101296.
21. Zhao S, Zhao Y, Zuo J, Le TS, Kerdsiri J, Waranuch N, et al. Evaluation of drug permeability across Ex vivo nasal mucosa: A simulation-based approach to minimize thickness-related variability. J Drug Deliv Sci Technol 2025;108:106959. https://doi.org/10.1016/j.jddst.2025.106959.
22. Trivedi S, Kause S, Belgamwar V. Intranasal delivery of poly (d-glucosamine) encrusted self-assembled lipidic nanovesicles to enhanced brain uptake of thymoquinone for management of Glioblastoma Multiforme. J Drug Deliv Sci Technol 2023;90:105149. https://doi.org/10.1016/j.jddst.2023.105149.
23. Singh PK, Srivastava AK, Dev A, Kaundal B, Choudhury SR, Karmakar S. 1, 3β-Glucan anchored, paclitaxel loaded chitosan nanocarrier endows enhanced hemocompatibility with efficient anti-glioblastoma stem cells therapy. Carbohydr Polym 2018;180:365–75. https://doi.org/10.1016/j.carbpol.2017.10.030.
24. Scudiero DA, Shoemaker RH, Paull KD, Monks A, Tierney S, Nofziger TH, et al. Evaluation of a soluble tetrazolium/formazan assay for cell growth and drug sensitivity in culture using human and other tumor cell lines. Cancer Res 1988;48:4827–33.
25. Fessi H, Puisieux F, Devissaguet JP, Ammoury N, Benita S. Nanocapsule formation by interfacial polymer deposition following solvent displacement. Int J Pharm 1989;55:R1–4. https://doi.org/10.1016/0378-5173(89)90281-0.
26. M Ways TM, Lau WM, Khutoryanskiy VV. Chitosan and Its Derivatives for Application in Mucoadhesive Drug Delivery Systems. Polymers (Basel) 2018;10. https://doi.org/10.3390/polym10030267.
27. Hassan AAA, Ramadan E, Kristó K, Regdon G Jr, Sovány T. Lipid-Polymer Hybrid Nanoparticles as a Smart Drug Delivery System

for Peptide/Protein Delivery. Pharmaceutics 2025;17. https://doi.org/10.3390/pharmaceutics17060797.
28. Danaei M, Dehghankhold M, Ataei S, Hasanzadeh Davarani F, Javanmard R, Dokhani A, et al. Impact of Particle Size and Polydispersity Index on the Clinical Applications of Lipidic Nanocarrier Systems. Pharmaceutics 2018;10. https://doi.org/10.3390/pharmaceutics10020057.
29. Illum L. Nasal drug delivery--possibilities, problems and solutions. J Control Release 2003;87:187–98. https://doi.org/10.1016/s0168-3659(02)00363-2.
30. Djupesland PG. Nasal drug delivery devices: characteristics and performance in a clinical perspective-a review. Drug Deliv Transl Res 2013;3:42–62. https://doi.org/10.1007/s13346-012-0108-9.
31. Mahapatro A, Singh DK. Biodegradable nanoparticles are excellent vehicle for site directed in-vivo delivery of drugs and vaccines. J Nanobiotechnology 2011;9:55. https://doi.org/10.1186/1477-3155-9-55.
32. Ali MS, Abdullah Almoyad MA, Wahab S, Sahebkar A, Gorain B, Kaur H, et al. Recent advances in lipid-based nanocarriers for advanced skin cancer therapy. Int J Pharm 2025;670:125203. https://doi.org/10.1016/j.ijpharm.2025.125203.
33. Nguyen T-T-L, Duong V-A. Advancements in Nanocarrier Systems for Nose-to-Brain Drug Delivery. Pharmaceuticals (Basel) 2025;18. https://doi.org/10.3390/ph18050615.
34. Dash S, Murthy PN, Nath L, Chowdhury P. Kinetic modeling on drug release from controlled drug delivery systems. Acta Pol Pharm 2010;67:217–23.
35. Costa P, Sousa Lobo JM. Modeling and comparison of dissolution profiles. Eur J Pharm Sci 2001;13:123–33. https://doi.org/10.1016/s0928-0987(01)00095-1.
36. Zhang Y, Huo M, Zhou J, Zou A, Li W, Yao C, et al. DDSolver: an add-in program for modeling and comparison of drug dissolution profiles. AAPS J 2010;12:263–71. https://doi.org/10.1208/s12248-010-9185-1.
37. Omidian H, Gill EJ, Dey Chowdhury S, Cubeddu LX. Chitosan Nanoparticles for Intranasal Drug Delivery. Pharmaceutics 2024;16. https://doi.org/10.3390/pharmaceutics16060746.